# Analysis of CO$_2$ Trapping Capacities and Long-Term Migration for Geological Formations in the Norwegian North Sea Using MRST-co2lab

Halvor Møll Nilsen, Knut-Andreas Lie, Odd Andersen

*SINTEF ICT, Department of Applied Mathematics, P.O. Box 124 Blindern, N–0314 Oslo, Norway*

**Abstract**

`MRST-co2lab` is a collection of open-source computational tools for modeling large-scale and long-time migration of CO$_2$ in conductive aquifers, combining ideas from basin modeling, computational geometry, hydrology, and reservoir simulation. Herein, we employ the methods of `MRST-co2lab` to study long-term CO$_2$ storage on the scale of hundreds of megatonnes. We consider public data sets of two aquifers from the Norwegian North Sea and use geometrical methods for identifying structural traps, percolation-type methods for identifying potential spill paths, and vertical-equilibrium methods for efficient simulation of structural, residual, and solubility trapping in a thousand-year perspective. In particular, we investigate how data resolution affects estimates of storage capacity and discuss workflows for identifying good injection sites and optimizing injection strategies.

*Keywords:* CO2 storage, Sleipner and Utsira, injection sites, rate optimization

## 1. Introduction

The net European CO$_2$ emissions from energy industries, manufacturing, and production totaled 1.95 Gt in 2011 according to the UNFCCC database[1]. Geological sequestration of a significant share of this CO$_2$ would require injecting hundreds of megatonnes underground annually. Altogether, the resulting storage requirement would be (at least) two orders of magnitude larger than the ongoing Sleipner injection or the planned White Rose project in the UK.

Sedimentary basins offshore Norway contain a number of saline aquifers with large volumes of pore space potentially usable for CO$_2$ storage. The Norwegian Petroleum Directorate has released two CO$_2$ Storage Atlases [1, 2] that explore large-scale CO$_2$ storage for a number of aquifers. In total, twenty-seven geological formations have been grouped into aquifers whose qualities are assessed with regard to CO$_2$ storage potential. Similar atlases have been compiled in other parts of the world [3, 4, 5, 6, 7]. See also [8] for a summary of sites and storage capacities for European countries.

Pressure buildup is often the main effect that limits storage capacity in closed or low-conductive aquifers, see e.g., [9, 10]. For open aquifers with good hydraulic conductivity, leakage risk due to long-term CO$_2$ migration could be a larger concern and one must therefore determine the amounts of CO$_2$ retainable by different trapping mechanisms. In most relevant scenarios, the injected CO$_2$ has lower density than the surrounding formation fluid, and will form a buoyant plume that might migrate long distances below a sealing, sloping caprock. Over time, some CO$_2$ will be retained in structural and stratigraphic traps (structural trapping), be trapped as small droplets between rock grains (residual trapping), dissolve into the formation water (solubility trapping), or react with rock minerals and become permanently trapped (mineral trapping). Simulating the trapping processes constitutes a challenging multiscale problem that is best attacked using a range of different computational approaches.

In [11, 12, 13], we describe an ensemble of simulation tools that can be used to simulate likely outcomes of large-scale, long-term migration processes and estimate capacity for structural, residual, and solubility trapping. These tools are implemented using a high-level scripting language and made publicly available as a separate module [14] of the open-source Matlab Reservoir Simulation Toolbox (MRST) [15, 16]. Herein, we demonstrate how these tools can be combined to provide alternative estimates of storage capacities. First, a set of simple geometrical/percolation type methods are employed to identify traps, accumulation areas, and spill paths [11] to provide upper bounds on the overall capacity for structural trapping. We analyze how the resulting estimates depend on the data resolution and then use vertical equilibrium (VE) models [17, 18, 19, 20, 21, 22, 23, 24, 25], whose efficient implementation is discussed in [12, 13], to provide practical and realistic estimates for representative storage scenarios in which CO$_2$ is injected at a finite rate. In VE models, the flow of a thin CO$_2$ plume is approximated in terms of its thickness underneath the top zeal of the aquifer to obtain a 2D simulation model. Although this reduces the dimension of the model, important information of the heterogeneities in the underlying 3D medium is preserved and the errors resulting from the VE as-

---

sumption are in many cases significantly smaller than those seen in (overly) coarse 3D simulation models. The presented examples are based almost entirely on publicly available data sets, and complete scripts can be downloaded and used under the GNU Public License version 3.

## 2. Impact of model resolution

The accuracy of geological models used to represent large saline aquifers will in most cases be questionable. First of all, there is a general lack of accurate data: seismic surveys are not as dense as for petroleum reservoirs, core data from drilling are scarce, etc. Secondly, because of the large spatial areas involved, standard 3D flow simulations can typically only be performed on relatively coarse models to be computationally tractable, see discussion in [26]. If we think of the top seal as an undulating surface, any oscillation with a wave length shorter than twice the cell size cannot be represented. Decreasing the resolution will typically remove a great number of smaller structural traps and tend to underestimate structural trapping capacity and retardation effects.

In the $CO_2$ Storage Atlas [1], twenty-one geological formations have been individually assessed and grouped into saline aquifers that can be considered candidates for $CO_2$ injection. Using information from the accompanying data sets, we were able to construct grid models and estimate structural trapping capacity for fourteen different sand volumes [11]. The atlas data sets cover large areas and are primarily intended for mapping. The extracted grid models are therefore comparatively coarse, with typical lateral resolutions of 500 or 1000 m. Moreover, inaccuracies are also introduced during the data integration process when constructing the simulation grids, as explained in [11]. In this section, we will discuss the impact of model resolution in more detail for two of the fourteen aquifers considered in [11].

### 2.1. The Johansen formation

The deep saline Johansen aquifer [27, 28, 29, 30] is located below the Troll field on the Southwest coast of Norway. The aquifer has an estimated theoretical storage capacity in the range of 1–2 billion tonnes of $CO_2$ and was proposed as a storage site for $CO_2$ to be captured from gas power plants at Mongstad and Kårsø.

In [11], we outline how the potential for structural trapping predicted by the atlas model of Johansen deviated significantly from two low-resolution (sector and field) models previously developed for simulation purposes [29]. Herein, we investigate the effect of model resolution by generating six grid realizations using raw data from the $CO_2$ Storage Atlas, see Figure 1. The first realization is the full data set with 500 m lateral resolution, the second is coarsened by a factor two in each lateral direction, the third by a factor three, and so on. All grids are fairly coarse compared to typical simulation grids. All major traps appear inside the domain and hence the estimates of trapping are not significantly affected by how the computational algorithm determines traps against the perimeter, which here is assumed to be open.

Table 1: Impact of grid resolution on structural trapping for the Johansen formation.

| Resolution [m] | # traps | Bulk volume [m$^3$] | Avg. volume [m$^3$] |
|---|---|---|---|
| 500 | 722 | 2.61e+10 | 3.62e+07 |
| 1000 | 154 | 2.67e+10 | 1.73e+08 |
| 1500 | 73 | 2.75e+10 | 3.76e+08 |
| 2000 | 41 | 2.41e+10 | 5.88e+08 |
| 2500 | 26 | 2.35e+10 | 9.04e+08 |
| 3000 | 21 | 2.23e+10 | 1.06e+09 |

Figure 2 and Table 1 show the result of an analysis of the structural trapping capacity for the six different grids. Note that several smaller traps are removed as the coarsening increases, which can be observed statistically by noting that the mean of the trap volume quickly increases as the smaller traps are smoothed away. Total trapping volume also changes as we coarsen the model: first, the volume increases as the largest traps become slightly larger due to the lower resolution. However, as the resolution further decreases, the total volume shrinks as smaller traps are removed entirely.

The general effect of coarsening is well studied within reservoir simulation, but the problem of $CO_2$ injection is special in that it contains a light $CO_2$ phase trapped above a nearly immobile water or hydrocarbon phase. Small-scale traps not only increase the volume available for structural trapping, but can significantly divert spill paths and retard plume migration and hence increase the volumes that can be injected and safely contained within the boundaries of an aquifer [31, 32, 24]. The geometry of the top surface can therefore in many cases have an effect on the total amount of trapped $CO_2$ that is larger than the effect of fine-scale permeability variations. In [12], we outlined several effective models that account for the retardation effect from unresolved caprock undulations. Data that can be used to estimate small-scale undulations in the top seal will usually not be available. In the next subsection, whoever, we will discuss a case in which such data *is* available.

### 2.2. The Utsira formation

The world's first commercial $CO_2$ storage project started in 1996 at the Sleipner West field on the Norwegian Continental Shelf. Here, $CO_2$ that is a byproduct from natural gas production is injected into the neighboring Utsira formation. The annual injection rate is approximately one metric megatonne of $CO_2$ per year. Six seismic surveys acquired between 1999 and 2008 indicate how the injected $CO_2$ has accumulated under a series of nine geological horizons [33], and there is no evidence so far of $CO_2$ leaking out of the formation.

Here, we will use geological models that have been developed for the ninth and upper horizon in the area around the injection site to illustrate and estimate the impact that data resolution has on the estimated trapping capacity for the whole Utsira formation. These models are:

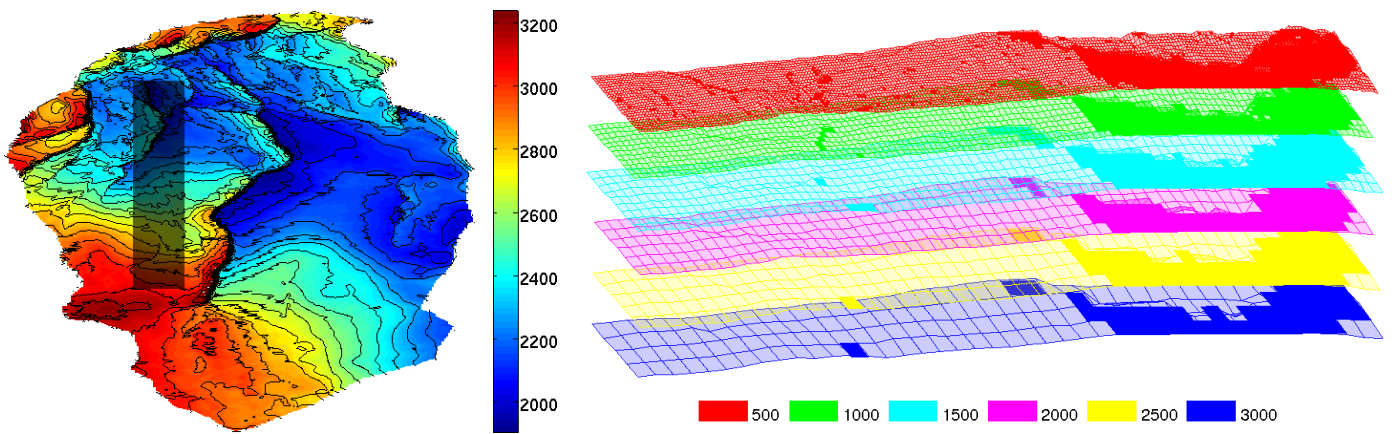**IEAGHG:** Sleipner model provided by IEAGHG [34], 50 m resolution;

2

Figure 1: Models of the Johansen aquifer from the $CO_2$ Storage Atlas covering an area of $45.8 \times 101.2$ km$^2$. The left plot shows the depth map in meter for the model with full lateral resolution of 500 m. The plot to the right shows the top surface for the $5 \times 50$ km$^2$ subregion marked in gray in the left plot for six different lateral resolutions. Cells that are inside traps are marked in solid color.
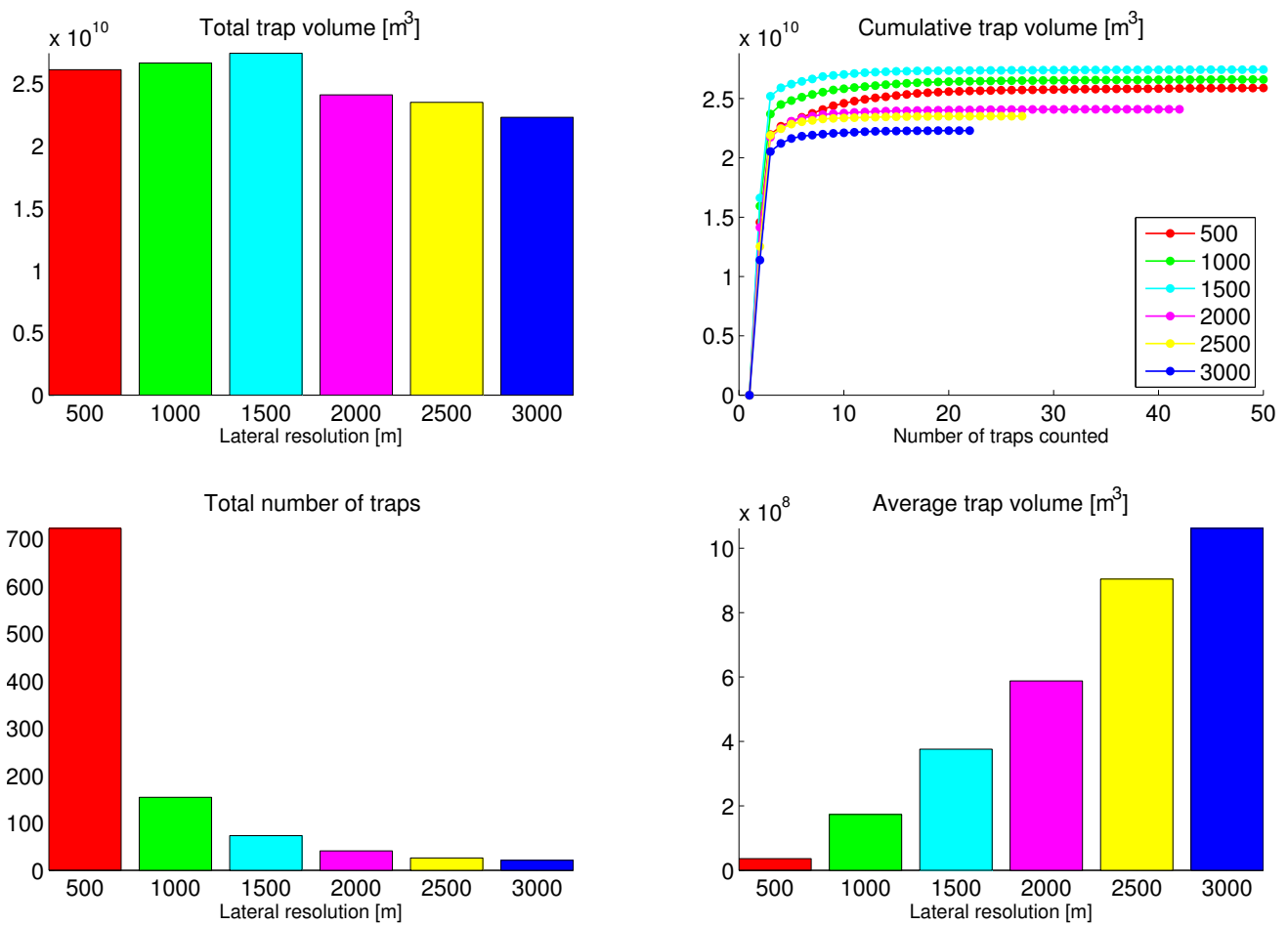


Figure 2: Impact of grid resolution on structural trapping capacity for the Johansen formation. For the cumulative plot, the traps have been sorted by volume in descending order.
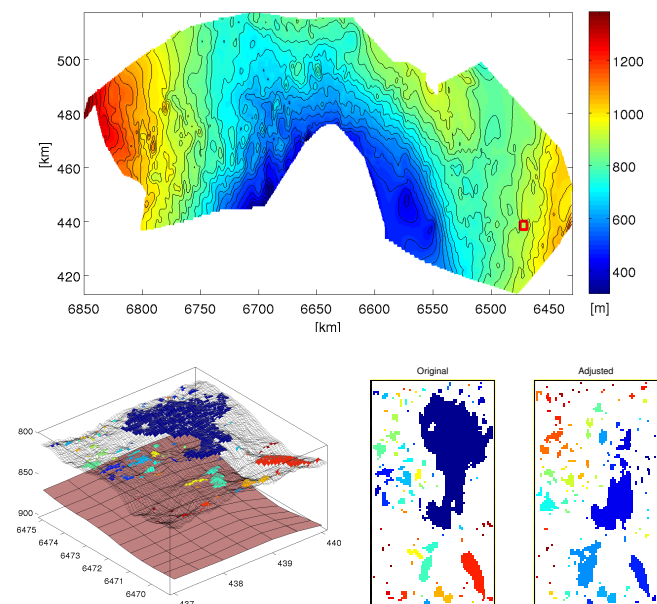
Figure 3: Estimation of sub-resolution trapping in the Utsira formation. The first plot shows the depth map of the Utsira atlas model with the IEAGHG model of Sleipner marked as a small red box. The next plot shows the IEAGHG surface (50 m) with color-coded traps plotted above the low-resolution Utsira model (500 m) of the same area. The last plots show structural traps on the original IEAGHG model (left) and on a version in which the height variations of the low-resolution Utsira model have been eliminated (right).

**GHGT:** in-house model used in [19], same resolution as the IEAGHG model but covers a larger region;

**INHOUSE:** in-house model from Statoil which covers the same region as the IEAGHG model, but with a 12.5 m resolution.

Comparing the structural trapping capacities derived from these models with the corresponding figure derived from the coarser (500 m resolution) Utsira model constructed from atlas data, we can estimate the amount of fine-scale structural trapping capacity that is not captured by the latter model.

Figure 3 compares the IEAGHG model with the corresponding region from the atlas model. What is seen as a smooth surface without any local maximum in the coarse atlas model will in the IEAGHG model contain a large number of structural traps of varying sizes. Altogether, the IEAGHG model predicts an average small-scale bulk trap volume of 560 liters per m$^2$. However, this simple analysis does not separate between truly sub-scale traps and those large enough to be reflected in the atlas grid. Indeed, part of the structural capacity described by the detailed model could still be represented by the coarser model. To avoid double-counting when estimating the amount of structural capacity only present in the detailed model, we base the analysis on the *difference* surface, obtained by subtracting the height variations of the atlas model from the IEAGHG model as shown to the left in Figure 4. We thereby obtain the fine-scale surface that only represents relative depth variations not resolved in the atlas model. This gives an average of 210 liters of unresolved trapping volume per m$^2$. Assuming that these local undulations are representative for the rest of the Utsira model, we predict
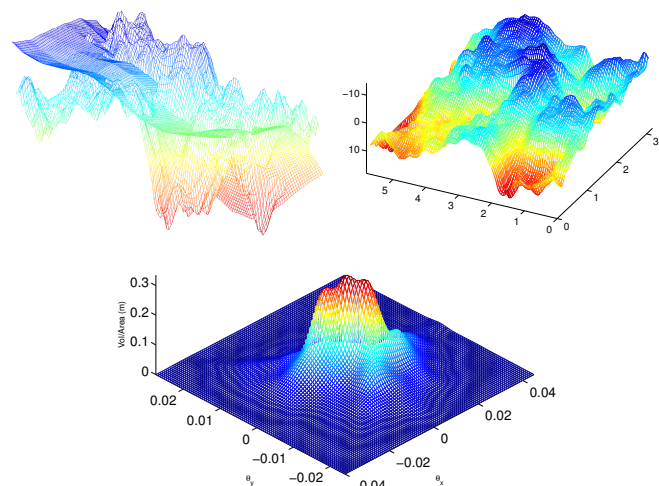


Figure 4: Estimation of small-scale trap volumes not resolved in the atlas model. *Top-left*: fine-scale interpolant from atlas data imposed on top of the IEAGHG model (scales exaggerated vertically), see also lower-left plot in Figure 3. *Top-right*: the corresponding residual surface. *Bottom:* average volume of sub-resolution traps per unit area as a function of the average tilt angle of the coarse surface.

the additional geometric trapping capacity from the fine-scale grid to be $5.1 \times 10^9$ m$^3$ across the model, which amounts to 30.5 % of the bulk volume of traps estimated directly from the original model.

The impact of the additional fine-scale structure relative to a flat, horizontal surface will likely exaggerate the local trapping effects; the volume of local traps obviously becomes smaller if the residual surface is imposed on an inclined, planar surface. To assess this effect, we give the residual surface a global tilt and compute the average volume of unresolved traps per surface area as a function of the angle and direction of inclination. The resulting function is shown to the right in Figure 4. We notice that the function is not symmetric, and that the maximum amount of trapping occurs for a nonzero tilt. This can likely be attributed to an inconsistency in the overall inclination angle of the high and low-resolution models. To compensate, we shift the maximum point to the origin. By assuming that the amount of sub-resolution trapping does not vary much across the formation, this function, which we refer to as the *sub-scale trapping function*, can be interpreted as an estimate of sub-scale trapping capacity per surface area as a function of local tilt and be used as input to the effective models outlined in [12].

The unresolved small-scale trapping potential for the whole Utsira formation can now be estimated as follows: for each cell in the atlas model, we calculate the local tilt angle and direction, and determine the corresponding unresolved trapping capacity by evaluating the sub-scale trapping function and multiplying by cell area. Doing this for all cells in the Utsira model and summing up, we obtain a global estimate of sub-scale trapping. We have constructed sub-scale trapping functions based on residual surfaces obtained by subtracting the atlas grid from the aforementioned IEAGHG, GHGT, and INHOUSE data sets. In addition, we constructed a sub-scale trapping function using a ver-

Table 2: Estimates of unresolved small-scale geometrical trapping as a percentage of resolved geometrical trapping for the atlas model of Utsira. Each column represents the result of using a particular estimate of the trapping function, based on the difference between the high-resolution and low-resolution surfaces indicated in the header. The slope-dependent estimate is computed taking local tilt into account, whereas the other estimate is obtained by assuming a constant tilt everywhere that maximizes sub-scale trapping for the local fine-scale model.

| High-resolution Low-resolution | IEAGHG Utsira | GHGT Utsira | INHOUSE Utsira | IEAGHG IEAGHG[1] |
|---|---|---|---|---|
| slope-dependent | 17.7% | 19.5% | 17.2% | 13.6% |
| constant | 55.3% | 59.4% | 55.9% | 45.3% |

[1] smoothed version of grid

sion of the IEAGHG top surface in which all details with resolution below 500 m were removed by smoothing with a Gaussian kernel. By computing the residual surface (and sub-scale trapping function) from one data set only, we obtain a trapping function that is not affected by inconsistencies between different data sets.

The results assuming a constant or slope-dependent amount of subscale trapping for each data set are presented in Table 2. From these figures, we estimate that the amount of sub-scale trapping not resolved in the atlas model is in the range of 13–20%. The large difference between the constant and the slope-dependent estimates shows that it is important to properly account for the interplay between the local slope and the steepness of the small-scale undulations in the caprock. How this interplay impacts upscaled relative permeabilities is discussed in detail in [25].

## 3. Sleipner: upscaled injection operation

We now use the Utsira aquifer model obtained from the $CO_2$ Storage Atlas to investigate the long-term fate of $CO_2$ for a hypothetical upsized operation at Sleipner. We consider an injection rate of 10 Mt per year (approximately ten times the actual injection rate), for an injection period of 50 years, followed by a 3000 year migration period. We run three simulations, which all include residual trapping, structural trapping, and sub-scale trapping (as estimated from the combined Sleipner and Utsira data sets in Section 2.2), but which differ in their treatment of solubility trapping. The first simulation does not include dissolution effects, the second simulation considers dissolution to be instantaneous in any vertical column where $CO_2$ is present, and the third simulation models a constant *rate* of dissolution, as explained in [12, 20]. Solubility of $CO_2$ in brine is assumed to be 53 kg/m$^3$ for the two latter simulations (taken from [35]), and the dissolution rate in the third simulation is set to 0.44 kg/m$^2$ per year. The simulations are performed using a fully-implicit VE simulator based on a sharp interface model, implemented using automatic differentiation. $CO_2$ density and viscosity values are functions of local pressure and temperature, computed using [36]. Linear compressibility is assumed for rock ($10^{-5}$ bar$^{-1}$) and brine ($4.3 \cdot 10^{-5}$ bar$^{-1}$). Residual saturation for brine and $CO_2$ are respectively set to 0.11 and 0.21, as suggested in [37]. We consider a uniform rock porosity of 21.1 percent, as inferred from [1].
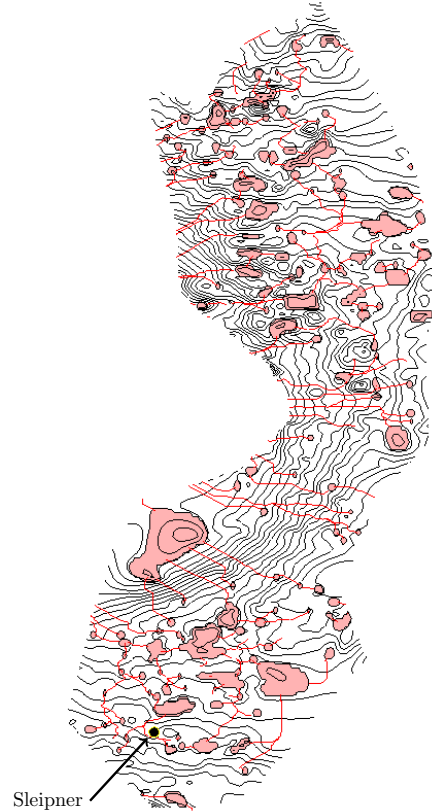


Figure 5: Map over structural traps and connecting spill paths for the Utsira formation.

### 3.1. Initial analysis of structural trapping potential

We first assess how much $CO_2$ we can expect to store in structural traps from the Sleipner injection point. Figure 5 presents a map of structural traps at Utsira, with the location of the Sleipner injection indicated. Altogether, these traps represent a combined pore volume of 3.55 km$^3$, which is 0.44% of the total pore volume of the aquifer model. Previous studies have arrived at roughly comparable figures. [39] estimates a total of 1.8 km$^3$ of pore space within structural closures of Utsira, extrapolated from analysis of 3D seismic data around the Sleipner area, whereas [40] arrives at a value of 1.10 km$^3$, based on multiplication of certain assumed ratios. The left plot of Figure 6 indicates the capacity of each identified structural trap in terms of $CO_2$ mass. The *cumulative* structural trapping along the length of the spill path from an injection point and to the top of the formation is presented in the middle plot. According to this figure, the cumulative trap capacity reachable from the Sleipner site is close to 30 Mt. On the other hand, the injection point is located close to a region with much higher reachable capacity (215 Mt). Since the real flow of $CO_2$ will be far from infinitesimal, and initially driven primarily by viscous forces, we expect that a considerable amount of $CO_2$ will end up there as well. If we add up the figures for the two regions, we conclude that we might to reach up to 245 Mt of structural capacity from the Sleipner injection point (not counting subscale trapping), or 49% of the total injected $CO_2$ during the operation. However, if
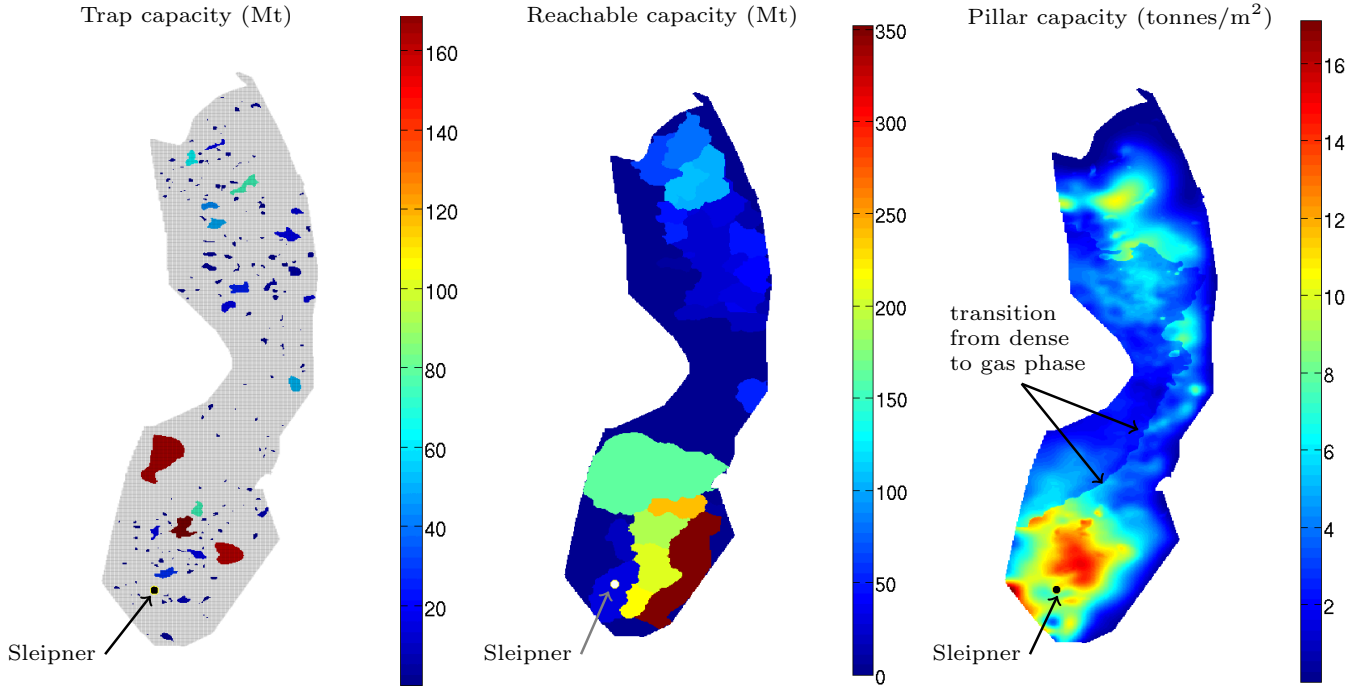
Figure 6: Analysis of trapping capacity for the Utsira formation. *Left*: Individual structural traps, color-coded by estimated $CO_2$ mass trapping capacity. *Middle*: Combined capacity of upstream traps that can be reach along a spill path from each point in the aquifer. The total structural capacity of the aquifer is 1.13 Gt [38]. *Right*: Total theoretical $CO_2$ retaining capacity per square meter, taking all trapping mechanisms (structural, residual, solubility) into account. The total containing capacity of the whole aquifer is 112 Gt [38].

we also consider the other trapping mechanisms (residual, solubility), we can hope to retain a significantly higher amount. The right plot of Figure 6 is a map of the estimated total trapping capacity per lateral square meter of the aquifer, taking structural, residual, and solubility trapping into account. This estimate is highly theoretical, since it considers an (unobtainable) one hundred percent sweep efficiency and complete saturation of dissolved $CO_2$ in formation water. However, the plot still indicates that the Sleipner injection point is located close to a region that is able to hold large amounts of $CO_2$ by a combination of trapping mechanisms. A detailed discussion of the assumptions and parameters behind the construction of this figure is presented in [38].

*Simulation results*

The outcomes of the three simulations are presented in Figures 7–9. For each simulation, three snapshots of the $CO_2$ distribution are presented, corresponding to year 50 (injection end), year 1085, and year 3050. We also present an inventory that details the various forms in which $CO_2$ is trapped as a function of time. The diagram uses a color coding that goes from dark green for volumes that are safely trapped to red for volumes that have escaped across the perimeter of the domain. In the diagram, and in the following discussion, we use the term *(movable) $CO_2$ plume* for regions in which the $CO_2$ saturation is higher than the residual saturation. When the $CO_2$ is present at residual or lower saturation, it is considered to be residually trapped. To distinguish volumes that can move and volumes that cannot, the mobile $CO_2$ plume is divided into a free part

that may continue to propagate in the upslope direction and a residual part that is destined to be left behind after imbibition as the movable plume propagates upslope. Likewise, the structurally trapped volumes are divided into a free part that may potentially leak through imperfections in the caprock and a residual part that is permanently immobilized and cannot escape the trap. The inventory also accounts for volumes that are immobilized within small traps not resolved by the simulation grid. Figure 10 provides a conceptual illustration and Table 3 summarizes the terminology.

In Figure 7, we note that at the end of simulation, approximately 75 Mt (15%) of the injected $CO_2$ has leaked from the domain. The onset of this leakage occurs after approximately 1400 years. After this period, little additional $CO_2$ becomes structurally or residually trapped, since flow is now predominantly along established pathways. This also means that most of the remaining 280 Mt of free $CO_2$ is likely to leak in the future. We note that at the end of simulation, approximately 70 Mt of $CO_2$ has become structurally trapped at the macro scale ("Structural residual" and "structural plume"). This means that in addition to the 30 Mt of reachable structural capacity identified in our initial analysis, approximately 40 Mt of $CO_2$ has been structurally trapped in the neighboring spill system, with an additional 25 Mt of $CO_2$ trapped in subscale traps ("structural subscale") that are not resolved on the grid. Altogether, the injection utilizes approximately 6% of the structural capacity of the resolved traps and 11–16% of the subscale trapping capacity estimated in Table 2. The reason these numbers are different is that the plume only connects a specific subset of all

6

Table 3: Explanation of terminology used in the $CO_2$ inventory of Figures 7, 8 and 9.

| State | Explanation |
|---|---|
| Dissolved | $CO_2$ trapped by dissolution into formation brine |
| Structural residual | $CO_2$ that is both structurally and residually trapped |
| Residual | Residually trapped $CO_2$ outside free plume and structural traps |
| Residual in plume | $CO_2$ still in the free-flowing plume, but destined to be left behind after imbibition |
| Structural subscale | $CO_2$ trapped in caprock structures too small to be represented by the grid |
| Structural plume | structurally but not residually trapped $CO_2$ |
| Free plume | $CO_2$ that is still free to migrate (i.e. part of the plume that is neither residually nor structurally trapped) |
| Exited | $CO_2$ that has left the simulated domain |

the structural traps, whereas subscale trapping will take place in all the area contacted by the plume. By and large, though, the most important trapping mechanism here is residual trapping, which accounts for roughly half of all injected $CO_2$ at the end of the simulation period.

In Figure 8 and Figure 9, we can see that solubility trapping quickly ends up dominating all other trapping mechanisms in the two simulations that include this effect. However, there are significant differences in end results between these two models. In the case of instant dissolution (Figure 8), the full impact of dissolution is present from the start. As a result, the movable $CO_2$ plume never grows large, and as it moves it is quickly dissolved and does not migrate far. On the other hand, since the brine below the plume is saturated with $CO_2$ at all times, no additional dissolution occurs in areas where the plume remains present. On the trapping distribution diagram, we thus see a notably reduced growth of the dissolved component after some 1000 years, as migration gradually stagnates.

The effect of rate-dependent dissolution, as presented in Figure 9, is notably different. Here, dissolution does not become the dominant effect until after approximately a thousand years, meaning that the $CO_2$ manages to spread much farther. As a result of the larger spatial extent of plume migration, a larger amount brine is exposed to $CO_2$ here than in the instantaneous dissolution model, allowing for a larger total amount of $CO_2$ to be dissolved before saturation is reached. Moreover, we observe that the residual saturation (green) never grows much despite significant plume migration, as it is constantly depleted due to the ongoing dissolution.

## 4. Utsira: large-scale industrial injection

The amount of $CO_2$ theoretically retainable in the Utsira formation by structural and residual trapping is estimated to be orders of magnitude above the amounts currently injected at Sleipner [38]. In the present example, we simulate a large-scale operation in which up to 1.5 Gt of $CO_2$ is injected by means of ten separate injection sites over a fifty year period, after which we track 3000 years of migration. Injector locations are chosen to maximize utilization of available structural trapping, with optimal injection rates subsequently determined using a nonlinear

optimization approach. For the simulation, we use the same fully-implicit numerical model and parameters as in Section 3. We include structural, residual, and subscale trapping, but not the effect of dissolution.

### Choosing injection locations

The Utsira formation being a high-permeability, open aquifer, we assume pressure buildup to be of minor concern, and choose injection sites solely based on reachable structural trapping, using the rapid, greedy algorithm described in [11]. Within target catchment areas, injection locations are chosen as far away as possible from the formation boundary. The result is presented in Figure 11, with wells numbered according to the order they were chosen by the algorithm. We note two primary clusters of wells, one in the north and one in the south. Only a single well is located in the narrow middle region, which provides only a small amount of structural trapping, as apparent from Figure 6.

### Setting injection rates

Since reachable structural capacity for each injection site has already been identified, division by total injection period gives an initial suggestion of injection rates. This estimate does not take residual trapping into account, nor does it acknowledge that $CO_2$ may spill out of the intended regions during injection and migration. More optimal injection rates can be obtained by taking these effects into account. To this end, we use a nonlinear optimization approach, made practical by our ability to run multiple, rapid simulation using the VE framework [12]. For the optimization, we define an objective function that equals the combined total amount of $CO_2$ injected, minus the amount of $CO_2$ leaked by the end of the simulation period weighted by a factor ten to strongly penalize injection of volumes that will leak back out. To compute the value of the objective function for a given set of rates, a full VE simulation is carried out. The gradient of the objective function can then be obtained by an adjoint method [41, 42], and the optimization problem is solved iteratively with gradient-based method. As a starting point for the optimization algorithm, we use injection rates obtained from the estimates of reachable structural capacity, as described above. We will refer to these rates as the "initial rates", and those obtained from optimization as the "optimized rates". These are presented in Figure 12. As can be seen from this figure, injection rates for most sites are adjusted significantly upwards after optimization, primarily attributable to the additional effect of residual trapping. On the other hand, the injection rate of site 6 has been adjusted down to almost zero. This is further discussed below.

### Simulation results

We first consider the scenario using the initial (unoptimized) injection rates. The result is presented in the left plot of Figure 13 (trapping distribution over time) and the upper row of Figure 14, presented similarly to Section 3. The total amount injected in this scenario is 887 Mt, which equals the estimated reachable trapping capacity from the injection sites. As can be
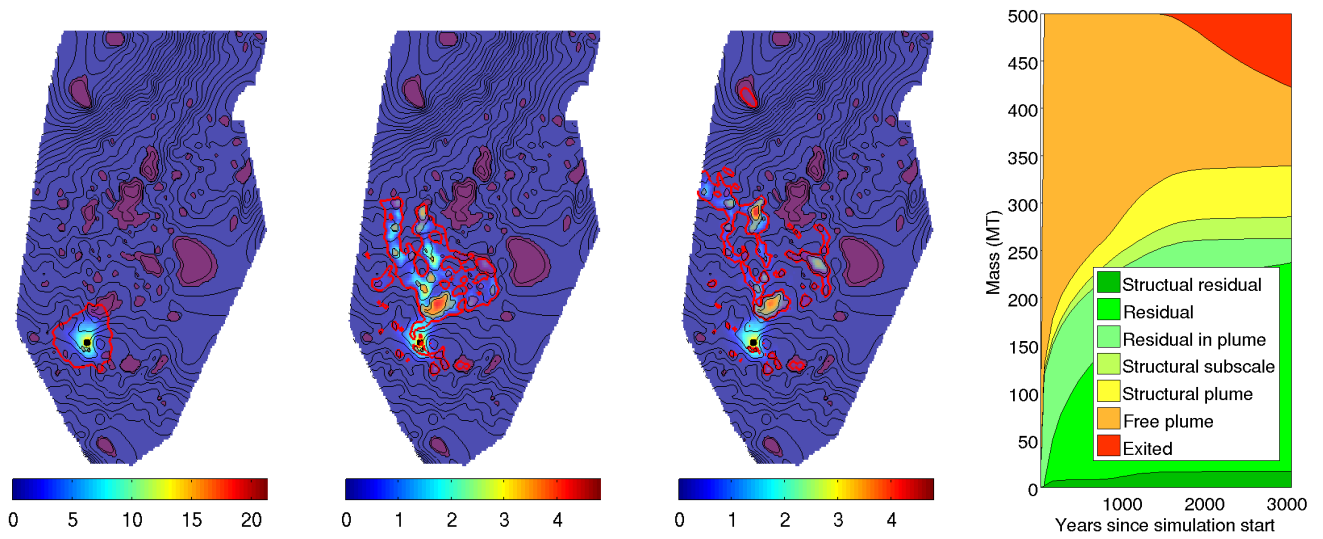
Figure 7: Simulation of single-point injection into the Utsira aquifer without dissolution effects. Snapshots of $CO_2$ distribution after 50, 1085, and 3050 years and diagram presenting historical trapping distribution. Outline of the remaining movable plume is traced in red, and overall $CO_2$ content of each vertical column indicated with color (unit: tonnes per lateral square meter). Structural traps indicated in purple.
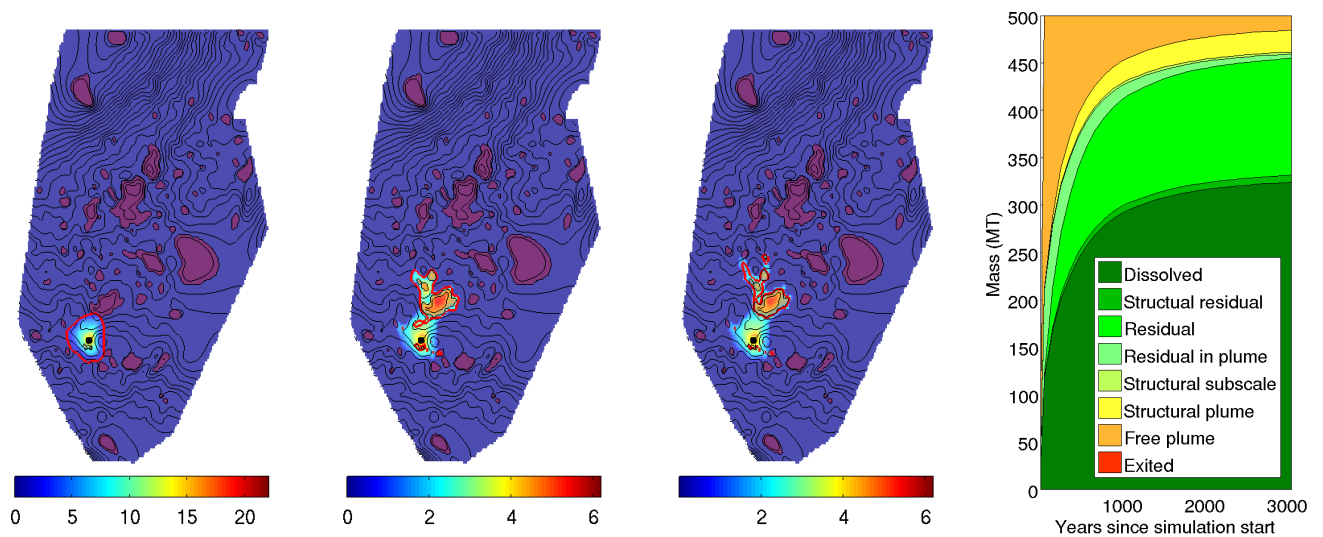


Figure 8: Simulation of single-point injection into the Utsira aquifer with instantaneous dissolution. Snapshots of $CO_2$ distribution after 50, 1085, and 3050 years.
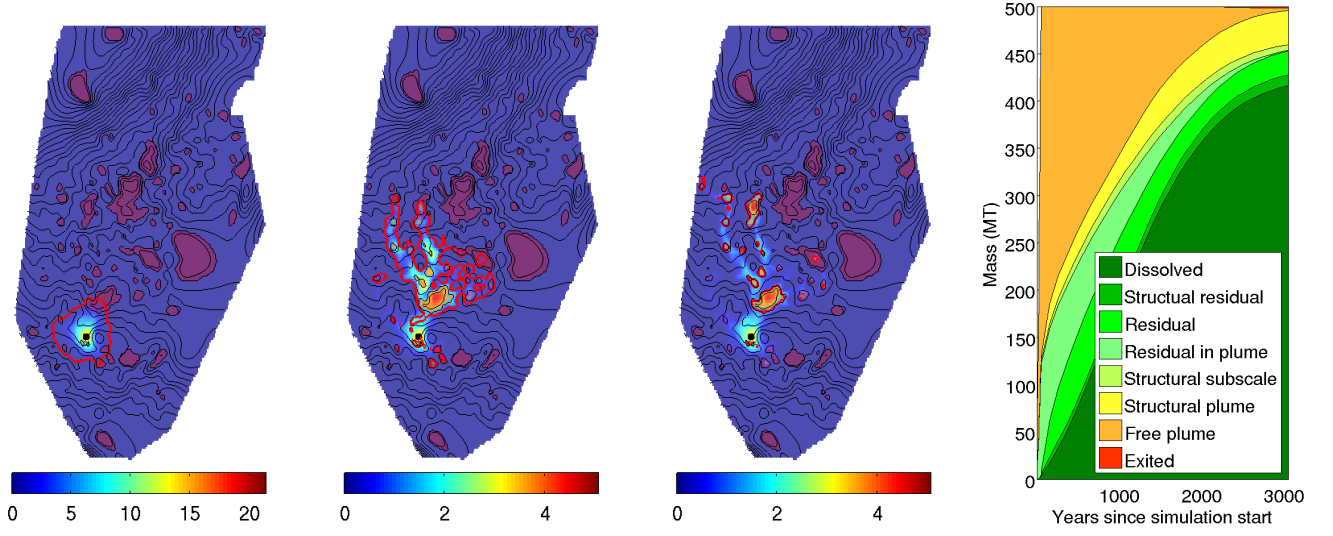
Figure 9: Simulation of single-point injection into the Utsira aquifer with rate-dependent dissolution. Snapshots of $CO_2$ distribution after 50, 1085, and 3050 years.
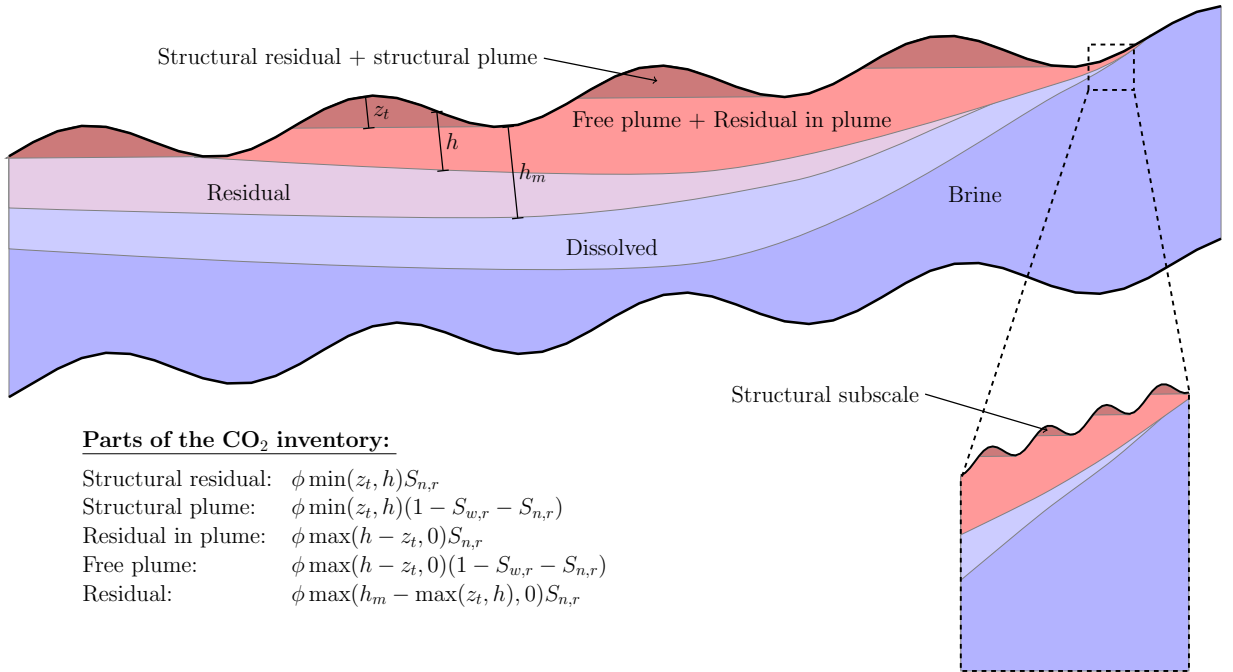


**Parts of the $CO_2$ inventory:**

| | |
|---|---|
| Structural residual: | $\phi \min(z_t, h) S_{n,r}$ |
| Structural plume: | $\phi \min(z_t, h)(1 - S_{w,r} - S_{n,r})$ |
| Residual in plume: | $\phi \max(h - z_t, 0) S_{n,r}$ |
| Free plume: | $\phi \max(h - z_t, 0)(1 - S_{w,r} - S_{n,r})$ |
| Residual: | $\phi \max(h_m - \max(z_t, h), 0) S_{n,r}$ |

Figure 10: Schematic of a vertical section of an aquifer identifying the various trapping states mentioned in Table 3. Here, $\phi$ is the pore volume, $S_{n,r}$ is the residual $CO_2$ saturation, $S_{w,r}$ is the irreducible water saturation, $z_t$ is the depth of the trap (or zero if there is not trap), $h$ is the depth of the movable plume, and $h_m$ is the largest depth at which $CO_2$ has been observed. The right inlet visualizes the small-scale undulations in the top surface that are not resolved by the large-scale model, thus accounted for as "subscale trapping" in our inventory.

9

seen from Figure 13, less than half of the injected $CO_2$ ends up in macro-scale structural traps ("structural residual" and "structural plume"), since significant amounts are retained by residual and subscale trapping. The leakage at the end of the simulation period is negligible, but approximately 10% of the $CO_2$ remains mobile and can potentially leak in the future. The simulation snapshots in Figure 14 illustrate how the $CO_2$ migration is generally upwards towards the the western boundary, with accumulation in encountered traps. Notably, a large part of the $CO_2$ injected from site 6 does not end up in the neighbor trap, but flows upwards along the steep slope towards the west.

The right plot of Figure 13 presents the trapping distribution over time for the simulation with optimized injection rates. In this simulation, a total of 1.52 Gt has been injected, still with negligible leakage at the end of the simulation period. The relative importance of the different trapping mechanisms remain comparable to the unoptimized case, but the relative amount of mobile $CO_2$ after 3000 years is approximately twice as large as before (approximately 300 Mt). A longer simulation period would allow a large part of this amount to eventually exit the domain. However, the objective function used in the optimization algorithm does not account for future developments, and does not penalize presence of mobile $CO_2$. What is considered "optimal" injection rates will therefore depend both on how much leakage is tolerated and on the considered time span. The corresponding simulation snapshots are presented in the lower row of Figure 14. We note that the migrating plumes have formed some established pathways towards the formation boundaries, where future leakage will take place. We also note that the amount injected from site 6 has been drastically reduced. As such, the amount of leaked $CO_2$ from this site has been reduced to a minimum, but the neighbor trap has ended up under-utilized. This is due to the placement of the injection site within the trap catchment area. As previously mentioned, the algorithm used to choose well sites favors positions at the edges of the targeted catchment area in order to maximize distance to the outer boundary. As a consequence, since real flow is neither infinitesimal nor purely gravity driven, some amount of $CO_2$ will spill out of the intended region. For site 6 in our example, this means that a large quantity of $CO_2$ takes the alternative path westwards rather than flowing into the intended trap. Since leakage is heavily penalized by our objective function, the result is that injection at this site is drastically scaled down. A more sophisticated algorithm for site selection would take into account the estimated radial extent of the plume after injection, and position the injection point far enough within the intended catchment area to minimize spill along unintended pathways.

As mentioned, the selection of sites are based on optimizing reachable structural capacity, assuming that pressure buildup is not a critical issue. To verify this assumption, we end our analysis by examining the overpressure attained during injection for the scenario with optimized injection rates, defined as the difference between initial (fluid-static) pressure and maximum pressure observed during the vertical-equilibrium simulation. We find that overpressure is highest at the earliest simulated time step, where it reaches 2.53 MPa. As can be
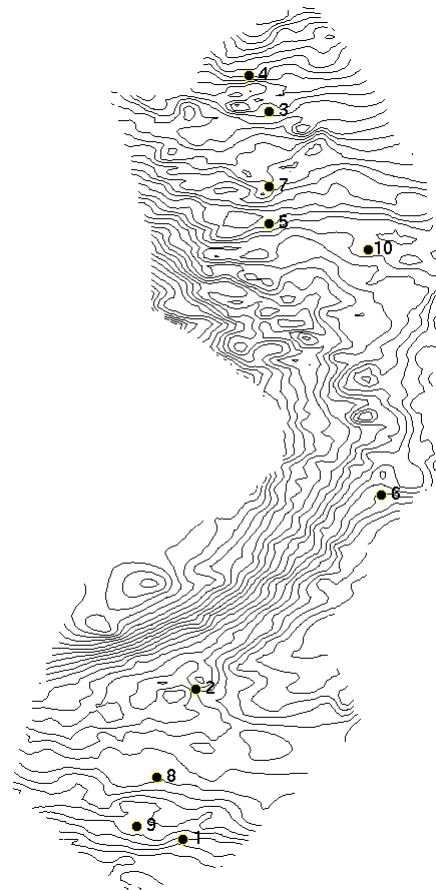


Figure 11: Choice of injection sites for large-scale utilization of the Utsira aquifer.

seen in Figure 15, this happens around the northernmost injection site, which is located in the deeper and thinner end of the formation. By assuming a lithostatic pressure gradient of 17 MPa/km [37], we estimate the Utsira overburden pressure to range from 4.8 MPa to 23 MPa depending on depth. We therefore conclude that in our simulated scenario, the overpressure from injection will at all times remain well below the overburden pressure. This conclusion would, however, strongly depend on the assumptions made about the aquifer boundaries, which were considered fully open. If we reduce the transmissibility of the aquifer boundary to mimic a situation where fluids expelled from the simulation domain have to pass through another 100 km of sandstone before reaching a hydrostatic pressure domain, our simulation produces a significantly higher overpressure of 4.12 MPa, now reached towards the end of the injection period. Similarly, running the same injection scenario with the assumption of fully closed boundaries yields an overpressure of 6.75 MPa. It is clear that any simulation of large-scale $CO_2$ storage at Utsira that intends to produce real figures on pressure buildup would require a valid model of the larger aquifer surroundings, and its effect on lateral fluid flow across aquifer boundaries as well as pressure-induced diffuse leakage of brine through the caprock.
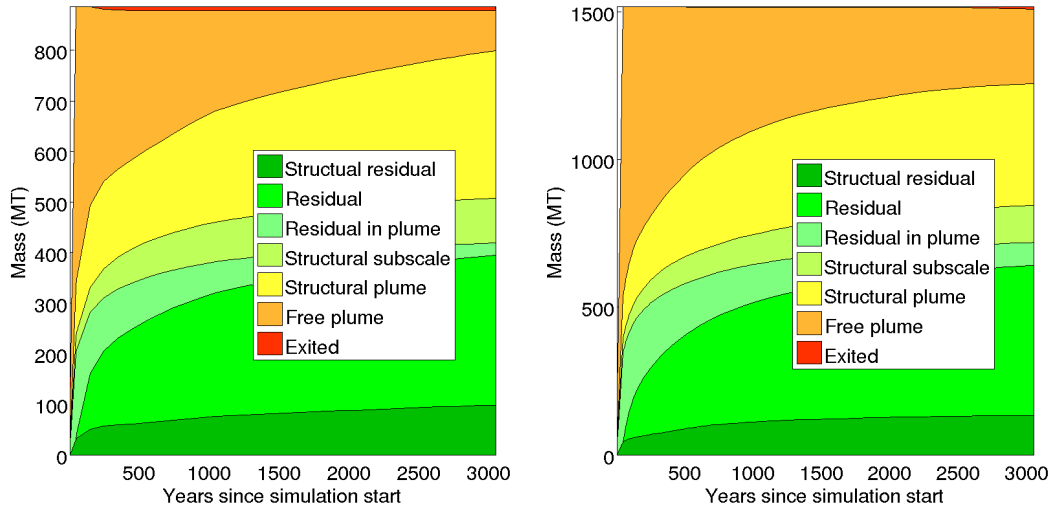
Figure 13: Historical trapping distribution of $CO_2$ for the scenarios presented in Section 4. The left diagram presents the history for the unoptimized case and the right diagram for the optimized case.
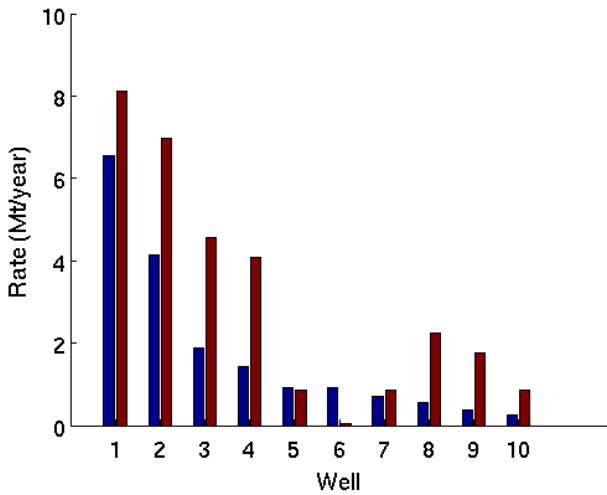


Figure 12: Initial (blue) and optimized (red) injection rates.

## 5. Concluding remarks

In this paper we have applied tools available in `MRST-co2lab` to process and analyze data sets available from the $CO_2$ atlases published by the Norwegian Petroleum Directorate. Our analyses include estimates on structural trapping potential, VE simulations to track $CO_2$ state and plume development, potential impact of subscale features and of dissolution, identification of good injection sites, and optimization of injection rates.

The use of VE models produces rapid results relative to the size of the targeted simulation problems. The low computational demand of such models is in part due to the reduced dimensionality of the simulated domain (from 3D to 2D) and in part due to weaker coupling of physical flow mechanisms. Although the reduction in dimensionality represents a significant simplification of reality, VE models still provide good results
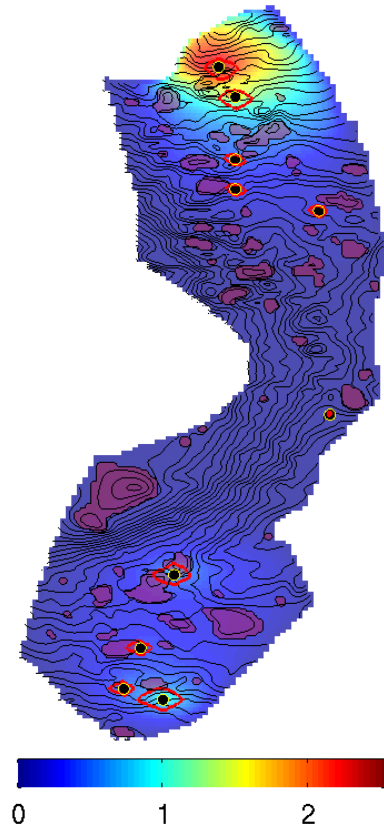


Figure 15: Overpressure at early injection stage for scenario with optimized injection rates for the Utsira aquifer (unit: MPa).
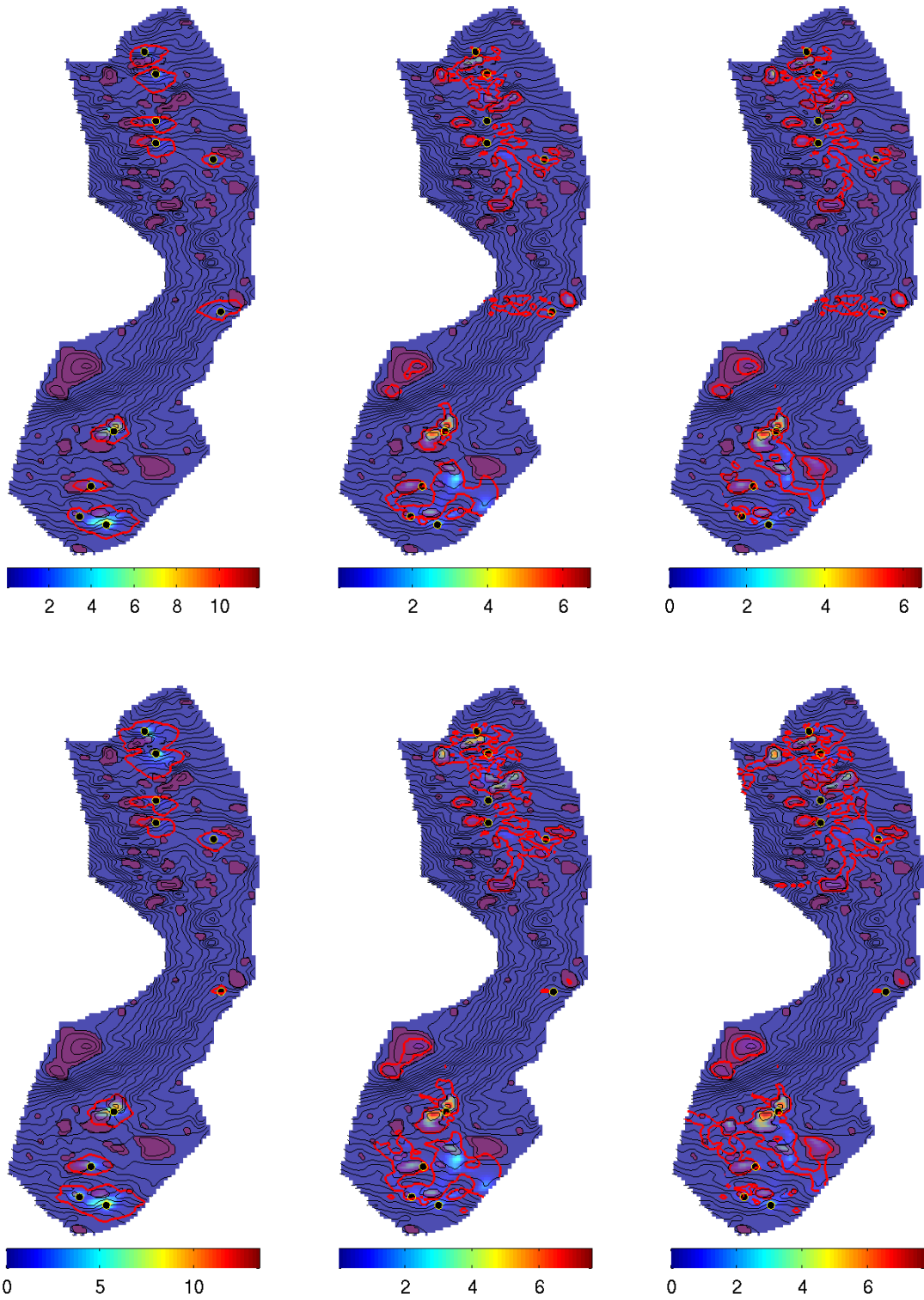
11

Figure 14: Simulation snapshots of the $CO_2$ distribution after 50, 1050, and 3000 years for the two injection scenarios presented in Section 4. The upper row presents the initial case with injection rates determined without flow simulation, while the lower row presents the optimized case. Outline of the remaining movable $CO_2$ plume is traced in red, and overall $CO_2$ content of each vertical column indicated with color (unit: tonnes per lateral square meter). Structural traps indicated in purple.

in many cases, and can take into account a range of physical phenomena. In the examples above, this includes hysteresis, subscale caprock variations, dissolution, and variable $CO_2$ density and viscosity as function of local temperature and pressure.

We strongly believe that rapid modeling tools can play an important role when evaluating capacity and performance of potential $CO_2$ storage sites, for designing usage scenarios, and for interpreting monitoring data after a site has become operative. The large scales involved and the limited availability and resolution of data means that obtaining definite forecasts from numerical simulations will likely remain an impossible task. However, the availability of rapid modeling tools makes it possible to extensively explore the unknown parameter space and thereby develop a good understanding of the various ways a given scenario *might* evolve, and identify scenario-specific important factors. The availability of rapid simulation tools also enables practical optimization of operational as well as physical parameters.

`MRST-co2lab` is published as an open-source module within MRST [15, 16]. Recognizing the importance of reproducible science, we have also made the numerical code behind the examples in this paper and its three predecessors publicly available [14]. The emphasis in `MRST-co2lab` is on rapid prototyping and exploration of ideas, and we believe it will support further advancement in the field both by presenting helpful tools for analyzing data sets, as well as providing a framework that allows researchers to quickly implement and test their ideas in terms of working code.

## Acknowledgments

## References

[1] E. K. Halland, W. T. Johansen, F. Riis (Eds.), $CO_2$ Storage Atlas: Norwegian North Sea, Norwegian Petroleum Directorate, P.O. Box 600, NO–4003 Stavanger, Norway, 2011.
URL http://www.npd.no/no/Publikasjoner/Rapporter/CO2-lagringsatlas/

[2] E. K. Halland, W. T. Johansen, F. Riis (Eds.), $CO_2$ Storage Atlas: Norwegian Sea, Norwegian Petroleum Directorate, P.O. Box 600, NO-4003 Stavanger, Norway, 2012.
URL http://www.npd.no/en/Publications/Reports/CO2-storage-altas-Norwegian-Sea/

[3] D. Lewis, et al., Assessment of the potential for geological storage of carbon dioxide for the island of Ireland, Tech. rep., Sustainable Energy Ireland, Environmental Protection Agency, Geological Survey of Northern Ireland, and Geological Survey of Ireland (2008).

[4] Natural Resources Canada, Mexican Ministry of Energy, and U.S. Department of Energy, The North American Carbon Storage Atlas (2012).
URL http://www.nacsap.org/

[5] U. S. Department of Energy, Office of Fossil Energy, The 2012 United States Carbon Utilization and Storage Atlas, 4th Edition (2012).
URL http://www.netl.doe.gov/research/coal/carbon-storage/atlasiv

[6] M. Cloete, Atlas on geological storage of carbon dioxide in South Africa, Tech. rep., Council for Geoscience, Johannesburg, South Africa (2010).
URL http://www.sacccs.org.za/wp-content/uploads/2010/11/Atlas.pdf

[7] B. E. Bradshaw, L. K. Spencer, A.-L. Lahtinen, K. Khider, D. J. Ryan, J. B. Colwell, A. Chirinos, J. Bradshaw, J. J. Draper, J. Hodgkinson, M. McKillop, An assessment of Queensland's $CO_2$ geological storage prospectivity–The Queensland $CO_2$ geological storage atlas, Energy Procedia 4 (0) (2011) 4583–4590, 10th International Conference on Greenhouse Gas Control Technologies. doi:10.1016/j.egypro.2011.02.417.

[8] EU GeoCapacity, Assessing European Capacity for Geological Storage of Carbon Dioxide, WP2 report: Storage capacity (2009).
URL http://www.geology.cz/geocapacity/publications/

[9] E. Lindeberg, J.-F. Vuillaume, A. Ghaderi, Determination of the $CO_2$ storage capacity of the utsira formation, Energy Procedia 1 (1) (2009) 2777–2784. doi:10.1016/j.egypro.2009.02.049.

[10] S. Thibeau, V. Mucha, Have we overestimated saline aquifer $CO_2$ storage capacities?, Oil Gas Sci. Technol. – Rev. IFP Energies nouvelles 66 (1) (2011) 81–92. doi:10.2516/ogst/2011004.

[11] H. M. Nilsen, K.-A. Lie, O. Møyner, O. Andersen, Spill-point analysis and structural trapping capacity in saline aquifers using `mrst-co2lab`, Computers & Geoscience 75 (2015) 33–43. doi:10.1016/j.cageo.2014.11.002.

[12] H. M. Nilsen, K.-A. Lie, O. Andersen, Robust simulation of sharp-interface models for fast estimation of $CO_2$ trapping capacity.
URL http://folk.uio.no/kalie/papers/co2lab-2.pdf

[13] H. M. Nilsen, K.-A. Lie, O. Andersen, Fully implicit simulation of vertical-equilibrium models with hysteresis and capillary fringe.
URL http://folk.uio.no/kalie/papers/co2lab-3.pdf

[14] SINTEF ICT, The MATLAB Reservoir Simulation Toolbox: Numerical $CO_2$ laboratory (Oct. 2014).
URL http://www.sintef.no/co2lab

[15] The MATLAB Reservoir Simulation Toolbox, version 2014a, http://www.sintef.no/MRST/ (May 2014).

[16] K.-A. Lie, S. Krogstad, I. S. Ligaarden, J. R. Natvig, H. M. Nilsen, B. Skaflestad, Open source MATLAB implementation of consistent discretisations on complex grids, Comput. Geosci. 16 (2012) 297–322. doi:10.1007/s10596-011-9244-4.

[17] J. M. Nordbotten, M. A. Celia, Geological Storage of $CO_2$: Modeling Approaches for Large-Scale Simulation, John Wiley & Sons, Hoboken, New Jersey, 2012.

[18] S. E. Gasda, J. M. Nordbotten, M. A. Celia, Vertical equilibrium with sub-scale analytical methods for geological $CO_2$ sequestration, Comput. Geosci. 13 (4) (2009) 469–481. doi:10.1007/s10596-009-9138-x.

[19] H. M. Nilsen, P. A. Herrera, M. Ashraf, I. Ligaarden, M. Iding, C. Hermanrud, K.-A. Lie, J. M. Nordbotten, H. K. Dahle, E. Keilegavlen, Field-case simulation of $CO_2$-plume migration using vertical-equilibrium models, Energy Procedia 4 (0) (2011) 3801–3808, 10th International Conference on Greenhouse Gas Control Technologies. doi:10.1016/j.egypro.2011.02.315.

[20] S. E. Gasda, J. M. Nordbotten, M. A. Celia, Vertically-averaged approaches to $CO_2$ injection with solubility trapping, Water Resources Research 47 (2011) W05528. doi:10.1029/2010WR009075.

[21] J. M. Nordbotten, H. K. Dahle, Impact of the capillary fringe in vertically integrated models for $CO_2$ storage, Water Resour. Res. 47 (2) (2011) W02537. doi:10.1029/2009WR008958.

[22] S. E. Gasda, J. M. Nordbotten, M. A. Celia, Application of simplified models to $CO_2$ migration and immobilization in large-scale geological systems, Int. J. Greenh. Gas Control 9 (2012) 72–84. doi:10.1016/j.ijggc.2012.03.001.

[23] F. Doster, J. M. Nordbotten, M. A. Celia, Hysteretic upscaled constitutive relationships for vertically integrated porous media flow, Comput. Visual. Sci. 15 (2012) 147–161. doi:10.1007/s00791-013-0206-3.

[24] S. E. Gasda, H. M. Nilsen, H. K. Dahle, W. G. Gray, Effective models for $CO_2$ migration in geological systems with varying topography, Water Resour. Res. 48 (10). doi:10.1029/2012WR012264.

[25] S. E. Gasda, H. M. Nilsen, H. K. Dahle, Impact of structural heterogeneity on upscaled models for large-scale $CO_2$ migration and trapping in saline aquifers, Adv. Water Resour. 62, Part C (0) (2013) 520–532. doi:10.1016/j.advwatres.2013.05.003.

[26] J. M. Nordbotten, B. Flemisch, S. E. Gasda, H. M. Nilsen, Y. Fan, G. E. Pickup, B. Wiese, M. A. Celia, H. K. Dahle, G. T. Eigestad, K. Pruess, Uncertainties in practical simulation of $CO_2$ storage, Int. J. Greenh. Gas Control 9 (0) (2012) 234–242. doi:10.1016/j.ijggc.2012.03.007.

[27] I. Akervoll, P. Bergmo, A study of Johansen formation located offshore

Mongstad as a candidate for permanent CO2 storage, in: European Conference on CCS Research, Development and Demonstration. 10–11 February 2009, Oslo, Norway, 2009.

[28] P. E. S. Bergmo, E. Lindeberg, F. Riis, W. T. Johansen, Exploring geological storage sites for CO2 from Norwegian gas power plants: Johansen formation, Energy Procedia 1 (1) (2009) 2945–2952. doi:10.1016/j.egypro.2009.02.070.

[29] G. Eigestad, H. Dahle, B. Hellevang, F. Riis, W. Johansen, E. Øian, Geological modeling and simulation of CO2 injection in the Johansen formation, Comput. Geosci. 13 (4) (2009) 435–450. doi:10.1007/s10596-009-9153-y.

[30] A. Sundal, J. P. Nystuen, H. Dypvik, R. Miri, P. Aagaard, Effects of geological heterogeneity on CO2 distribution and migration – a case study from the Johansen Formation, Norway, Energy Procedia 37 (2013) 5046–5054, 11th International Conference on Greenhouse Gas Control Technologies. doi:10.1016/j.egypro.2013.06.418.

[31] H. M. Nilsen, A. R. Syversveen, K.-A. Lie, J. Tveranger, J. M. Nordbotten, Impact of top-surface morphology on CO2 storage capacity, Int. J. Greenh. Gas Control 11 (0) (2012) 221–235. doi:10.1016/j.ijggc.2012.08.012.

[32] A. R. Syversveen, H. M. Nilsen, K.-A. Lie, J. Tveranger, P. Abrahamsen, A study on how top-surface morphology influences the storage capacity of $CO_2$ in saline aquifers, in: P. Abrahamsen, R. Hauge, O. Kolbjørnsen (Eds.), Geostatistics Oslo 2012, Vol. 17 of Quantitative Geology and Geostatistics, Springer Netherlands, 2012, pp. 481–492. doi:10.1007/978-94-007-4153-9_39.

[33] F. C. Boait, N. J. White, M. J. Bickle, R. A. Chadwick, J. A. Neufeld, H. E. Huppert, Spatial and temporal evolution of injected CO2 at the Sleipner Field, North Sea, J. Geophys. Res. B 117 (B3). doi:10.1029/2011JB008603.

[34] International Energy Agency, Sleipner benchmark model (2012).
URL http://www.ieaghg.org/index.php?/2009112025/modelling-network.html

[35] A. Chadwick, R. Arts, C. Bernstone, F. May, S. Thibeau, P. Zweigel, Best practice for the storage of CO2 in saline aquifers – Observations and guidelines from the SACS and CO2STORE projects, Vol. 14 of British Geological Survey Occasional Publication, British Geological Survey, Nottingham, UK, 2008.
URL http://nora.nerc.ac.uk/2959/

[36] I. H. Bell, J. Wronski, S. Quoilin, V. Lemort, Pure and Pseudo-pure Fluid Thermophysical Property Evaluation and the Open-Source Thermophysical Property Library CoolProp, Ind. Eng. Chem. Res. 53 (6) (2014) 2498–2508. doi:10.1021/ie4033999.

[37] V. Singh, A. Cavanagh, H. Hansen, B. Nazarian, M. Iding, P. Ringrose, Reservoir modeling of $CO_2$ plume behavior calibrated against monitoring data from Sleipner, Norway, in: SPE Annual Technical Conference and Exhibition, 19-22 September 2010, Florence, Italy, 2010. doi:10.2118/134891-MS.

[38] O. Andersen, H. M. Nilsen, K.-A. Lie, Reexamining $CO_2$ storage capacity and utilization of the Utsira Formation, in: ECMOR XIV – $14^{th}$ European Conference on the Mathematics of Oil Recovery, Catania, Sicily, Italy, 8-11 September 2014, EAGE, 2014. doi:10.3997/2214-4609.20141809.

[39] R. A. Chadwick, P. Zweigel, U. Gregersen, G. A. Kirby, S. Holloway, P. N. Johannessen, Geological reservoir characterization of a CO2 storage site: The Utsira Sand, Sleipner, northern North Sea, Energy 29 (910) (2004) 1371–1381. doi:10.1016/j.energy.2004.03.071.

[40] R. Bøe, C. Magnus, P. T. Osmundsen, B. I. Rindstad, Co2 point sources and subsurface storage capacities for co2 in aquifers in norway, NGU Report 2002.010, Geological Survey of Norway, N–7441 Trondheim, Norway (2002).
URL http:www.ngu.no/FileArchive/101/2002_010_skjerm.pdf

[41] X. Raynaud, S. Krogstad, H. M. Nilsen, Reservoir management optimization using calibrated transmissibility upscaling, in: ECMOR XIV – $14^{th}$ European Conference on the Mathematics of Oil Recovery, Catania, Sicily, Italy, 8-11 September 2014, EAGE, 2014. doi:10.3997/2214-4609.20141864.

[42] J. D. Jansen, Adjoint-based optimization of multi-phase flow through porous media – a review, Computers & Fluids 46 (1, SI) (2011) 40–51. doi:10.1016/j.compfluid.2010.09.039.